Icarus 347 (2020) 113810

Contents lists available at ScienceDirect

Icarus

journal homepage: www.elsevier.com/locate/icarus

Vacuum sintering behavior and magnetic transformation for high-Ti type basalt simulated lunar regolith

Lei Song [a], Jiao Xu [a,*], Hong Tang [b], Jiquan Liu [a], Jianzhong Liu [b], Xiongyao Li [b], Shuqian Fan [a,*]

[a] Chongqing Key Laboratory of Additive Manufacturing Technology and System, Chongqing Institute of Green and Intelligent Technology, Chinese Academy of Sciences, No.266 Fangzheng Avenue, Beibei District, Chongqing 400714, PR China
[b] Center for Lunar & Planetary Sciences, Institute of Geochemistry, Chinese Academy of Sciences, 99 Lincheng West Road, Guiyang 550081, PR China

ARTICLE INFO

Keywords:
Moon, surface
Regoliths
Experimental techniques
Mineralogy

ABSTRACT

Lunar regolith in-situ utilization receives increasing attentions due to development of lunar exploration research. The complex composition of lunar regolith leads to its complicated phase reaction and composition evolution at high temperature, whereas few studies focus on the alteration of physicochemical properties for simulated lunar regolith at high temperature. This paper focuses on physicochemical variation characteristics and magnetic transformation for high-Ti type basalt lunar regolith simulant CLRS-2 during vacuum sintering process. Importantly, the effect of heat-treatment on magnetic properties of CLRS-2 and the magnetic properties difference between high-Ti and low-Ti type basalt lunar regolith simulant have been investigated. The results would help us understand how the micro-morphology and chemical composition of ilmenite change in lunar regolith during sintering process. What can be inferred is that the ions substitution between ilmenite and other minerals or amorphous phase would occur during sintering process of lunar regolith at high temperature in vacuum, which would lead to the evaporation of Fe-containing components. Besides, the results of micro-hardness indicate that the ilmenite content difference between CLRS-1 and CLRS-2 have no influence on the micro-hardness of the sintered samples, while the density of samples and the sintering condition such as temperature have a greater influence.

1. Introduction

Plans for long-term lunar outposts require an imperative lunar base, which requires a lot of building materials, to sustain survival of humans. In consideration of the high cost of transporting between the Moon and the earth, the development for in situ resources utilization (ISRU) technology on the Moon is very critical for lunar base construction (Kawamoto and Shirai, 2012). The lunar regolith, covering on the Moon surface, is the most economical and feasible materials to build lunar bases or for other in situ utilization purposes such as carbothermal reduction and molten phase electrolysis to produce oxygen (Goulas et al., 2019; Gustafson et al., 2009; Colson and Haskin, 1992). In our opinion, the utilization of lunar regolith has derived from the building requirement and will finally thrive in various functional application demands on the Moon. Thus, adequate discussion on material properties for functional applications of lunar regolith and its simulants are quite necessary. Besides, the ISRU forming technologies for lunar regolith are urgently required. However, the forming mechanisms such as sintering properties for lunar regolith are still unclear, which greatly restricts the development of ISRU technology.

Over 60 years of spacecraft exploration has revealed that lunar regolith is mineralogically dominated by a combination of five minerals (plagioclase, orthopyroxene, clinopyroxene, olivine and ilmenite ($FeTiO_3$)), although the proportions of these minerals differ in different area (Slyuta, 2014; Schreiner et al., 2016; Crawford, 2015; Li et al., 2019). The amount of lunar regolith brought back to the earth by Apollo Missions can hardly meet the large demand of scientific research and engineering. Hence, a variety of simulant lunar regolith based on the Apollo samples came into being, such as JSC series, DNA-1, FJS-1, OB-1 and CLRS series which were developed by America, Europe, Japan, Australia and China (Taylor et al., 2016; Hintze and Quintana, 2013). However, even the Apollo samples are different from each other based on the collection position. And the actual landing point and the Moon stronghold coordinate position are quite unpredictable at present. Hence, the insight in the properties and possible applications for different lunar regolith simulants are quite necessary. The main Fe/Ti-

* Corresponding authors.
E-mail addresses: xujiao@cigit.ac.cn (J. Xu), fansq@cigit.ac.cn (S. Fan).

https://doi.org/10.1016/j.icarus.2020.113810
Received 9 July 2019; Received in revised form 25 March 2020; Accepted 6 April 2020
Available online 13 April 2020
0019-1035/

bearing phase in lunar rocks is the mineral ilmenite and the high-Ti basalts are mostly confined to lunar mare regions (Crawford, 2015). Chinese CLRS series lunar regolith simulants CLRS-1 and CLRS-2 are typical low-Ti and high-Ti type basalt lunar regolith simulants separately with different ilmenite contents. Actually, the contents of Ti and Fe for CLRS-2 are about 15%–20%, and they existed in the form of ilmenite which can be negligible in CLRS-1. Besides, CLRS-2's glass phase content is about 20–25%, which is much lower than 50–60% of CLRS-1.

Many forming technologies by sintering for simulating lunar regolith have been reported, including microwave sintering (Taylor and Meek, 2004), laser sintering (Goulas et al., 2019), solar sintering (Meurisse et al., 2018) and conventional sintering (Song et al., 2019). As known, the reactions during high-temperature forming process are complex and will greatly affect the forming process of multiphase lunar regolith simulants, for instance, our group has found the amorphous phases and forsterite had complex phase variation and reaction in the vacuum sintering of low-Ti type basalt lunar regolith simulant CLRS-1 (Song et al., 2019) and the final appearance of sintered bodies was different with temperature due to the reactions were varied with sintering temperature. Besides, Bischoff et al. have studied the nature of the lithiation process that converted loose regolith material into consolidated breccias which confirmed the role of feldspathic melt in consolidation process (Bischoff et al., 1984), and Hintze et al. have illustrated that there are diversities of sintering and melting temperature and mineral melting sequence of different lunar simulants during sintering process (Hintze and Quintana, 2013). Thus, the study of minerals components, phase transition and physicochemical reactions during sintering process is conducive to the correct selection of sintering temperature range and improvement of sintering forming technology for lunar regolith utilization. Obviously, it can be inferred that the difference of ilmenite contents may affect the sintering characteristics of basalt simulated lunar soil due to the complex sintering behavior of minerals at high temperature. Furthermore, the valence state of transition metal element Fe is prone to change due to its characteristics of electron arrangement in the outer layers of atom. Fe-containing minerals will have different complex changes when sintered at high temperature under different conditions, such as vacuum and air atmosphere (Song et al., 2019), which means Fe-containing minerals may have an important influence on sintering characteristics of simulated lunar regolith. Thus, in this paper, we will focus on the ilmenite composition influence for vacuum sintering of lunar regolith simulants.

In addition, it is reported that Fe in lunar regolith exists mostly in the form of Fe^{2+} or Fe^{0} owing to the high vacuum and anoxic environment on the surface of Moon (Forster, 1973), while a large amount of Fe in simulated lunar regolith, which are made up of earth minerals, is Fe^{3+}. As reported, the simulated and real lunar regolith both exhibit certain ferromagnetism, however, the former due to the presence of Fe^{3+}, while the latter mostly due to the presences of metallic iron (Rochette et al., 2010), including nano-metallic irons which only about 2% in weight at best (Taylor and Meek, 2004; Forster, 1973; Nagata et al., 1970), iron in iron–nickel mineral kamacite (Garrick-Bethell and Weiss, 2010) and high nickel taenite (Goldstein et al., 2009). Besides, 0.01–0.04 wt% Fe_3O_4 which could be products of lunar fumarolic activity or extra-lunar hydration and oxidation (Forster, 1973; Williams and Gibson, 1972). Based on previous studies (Goldstein et al., 2009; Nagata et al., 1971), we can infer that, in the high vacuum environment on the Moon, the lunar soil would remain ferromagnetic after undergoing melting process and solidification process, because the metallic iron could be crystallized in the form of ferroalloy minerals or elemental iron. However, it is still unknown how the ferromagnetism of simulated lunar regolith changes after sintering. What is known is that ilmenite normally belongs to trigonal system for $R\overline{3}$ space group, which is a complex solid solution based on the lattice of antiferromagnetic metatitanic ferrum ($FeTiO_3$). Exsolution of solid solution in ilmenite induces creation of titanomagnetite with spinel structure that distributes along (111) planes in ilmenite in the form of lamellar crystals and discontinuous arrangement along (0001) direction of ilmenite, which lead to weak ferromagnetic of ilmenite (Hong et al., 2012). That is to say, the ferromagnetism of CLRS-2 is mainly attributed to the exsolutions in ilmenite and different from the low-Ti type basalt simulated lunar regolith CLRS-1 which mainly due to the magnetite. By studying the magnetism change during sintering process of simulated lunar regolith, on the one hand, we can investigate the characteristics of iron-bearing minerals, especially ilmenite, in the process of high-temperature sintering by combining with other characterization methods. Besides, morphology, grain size and element distribution have a non-negligible influence on magnetic properties of simulated lunar regolith for its multiphase material system, and the change of composition during sintering process can relate to the change of magnetism. Thus, study on ferromagnetic change of high-Ti type basalt simulated lunar regolith could help us to infer how ilmenite changes in the complex system of real lunar regolith, although ilmenite in the lunar regolith is antiferromagnetic. On the other hand, the study on high temperature sintering of ferromagnetic minerals has an important reference value for utilization of high temperature sintered the mineral systems that rich in magnetite and ilmenite, such as Martian regolith which is rich in ferromagnetic minerals: magnetite and titanium inter-metallics such as titanomagnetite or titanomaghemite (Coey et al., 1990; Hargraves et al., 1979). For instance, ceramic/glass ceramic magnets for use in electronic equipment may be prepared by sintering of magnetic Martian regolith (Ramachandran et al., 2004). Furthermore, considering that people will rely on these artificially-prepared lunar regolith simulants for forming technology, device and mechanism research for many years to come, figure out the sintering properties and physical properties, such as magnetism, of different lunar regolith simulants are meaningful for lunar regolith utilization in the future and beneficial to comprehensive consideration for the landing point selection for in situ lunar soil utilization in the future, for instance, geological condition of the Moon surface and the difficulty of lunar base construction.

Thus, this paper will focus on the ilmenite influence on the evolution of composition, micromorphology and magnetic properties of CLRS-2 lunar regolith simulant during sintering processing under vacuum. The magnetic properties evolution for basalt simulated lunar regolith induced by the ilmenite amount in systems during sintering process was also analyzed. In addition, the micro-hardness of sintered samples was also measured to evaluate the possibility of its application in building materials or other applications. The composition heterogeneity and sintering condition impact on sintered simulated lunar regolith can be demonstrated by the results of micro-hardness.

2. Experimental

The lunar regolith simulant used in this research was the Chinese national standard sample high-titanium lunar simulant CLRS-2 (GSB 01-2187-2008) supplied by Institute of Geochemistry, Chinese Academy of Sciences. The lunar simulant with a relatively wide particle size and were obtained by grinding and crushing form volcanic ash from Jinchuan, Huinan, and the wall rock gabbro of vanadium-titanium magnetite deposit in Panzhihua with ratio of 1:2 (Yang et al., 2014). CLRS-2 with a sharp and irregular shape (Fig. 1S) is composed by 20–25% mafic volcanic glass, 15–20% Fe-Ti oxides and other minerals including pyroxene, feldspar and olivine, which is very similar to the actual lunar regolith sample collected from the lunar surface retrieved by the Apollo missions. Measured XRF results shown in Table 1 indicate that Si, Fe, Al, Ca, Mg and Ti are the main elements of CLRS-2, which is derived from volcanic vitreous, plagioclase, pyroxene, olivine and ilmenite (Zheng et al., 2004). To study the effect of ilmenite on composition evolution of CLRS-2 lunar simulant, ilmenite powder with a particle size of no larger than 200 mesh (≈74 μm) come from vanadium-titanium magnetite deposit in Panzhihua were used and the

Table 1
Composition (wt%) of the major constituents in lunar simulant CLRS-2 measured by XRF.

Chemical composition	SiO_2	Fe_2O_3	Al_2O_3	CaO	MgO	TiO_2	Na_2O	K_2O
Content (wt%)	45.62	14.52	12.16	9.99	7.19	5.47	2.59	1.03

powder was treated in the same way as that of CLRS-2. The melting points of CLRS-2 and ilmenite powders have been measured by Differential Scanning Calorimeter (DSC) and shown in Fig. 2S are 1152 °C and 1274 °C, respectively.

The dried simulated lunar regolith CLRS-2 powder of 0.6 g was placed in a cylindrical stainless steel mold with the inner diameter of 20 mm was compressed under 24 MPa pressure, and then kept this pressure for 4 min to form a disc shape green body as shown in Fig. 3S (a) with a thickness of about 1 mm. The green bodies placed on Al_2O_3 substrates were sintered in a commercial tube type vacuum sintering furnace (BTF-1200C, BEQ, China) with Edwards vacuum pump (RV8) to provide with vacuum condition. Details of sintering process and experimental procedure have been described elsewhere (Song et al., 2019). Simply, after the vacuum degree was reached to 2.0–5.0 × 10^{-3} mbar, the disc samples were heated with the heating rate of 15 °C·min^{-1} and then separately held at 600, 700, 800, 900, 1000, 1100 and 1150 °C in vacuum for 15 min. Then, the magnetic properties of heat-treated samples were determined by low temperature integrated physical property measurement system (PPMS DynaCool 9, Quantum Design, America), the measurement was carried out at room temperature (300 K), and the maximum magnetic field intensity was 1.5 T. Differential scanning calorimeter analysis (DSC) was performed using an STA 449 F3 apparatus (Netzsch, Germany) at a heating rate of 10 °C·min^{-1} from 100 °C to 1300 °C in air atmosphere. Micro-hardness of samples was measured using Full-automatic Vivtorinox hardness tester (AHVD-1000XY, SIOMM, China) under 500 gram-force and pressure keeping time of 15 s. Each sample was measured at three points.

3. Results

3.1. The magnetic study

The magnetic hysteresis loops of green body and sintered lunar regolith simulants CLRS-2 and CLRS-1 samples at room temperature have been measured and plotted in Fig. 1 and Fig. 4S, and the inset in Fig. 1 shows the magnified image of hysteresis loops center. The hysteresis loops of two kinds of simulated lunar regolith mostly exhibit weak ferromagnetic characteristic under 1.5 T. In addition, the hysteresis loops of 1150 °C CLRS-2 sintered sample is not completely symmetrical as shown in the inset which likely be caused by antiferromagnetic components in the samples such as Panzhihua ilmenite with both antiferromagnetic and ferromagnetic property (Hoffmann, 2004).

To be specific, the hysteresis loop area of CLRS-2 samples decreased with increasing of heat-treatment temperature when heat-treatment temperature below 1150 °C which means that the hysteresis loss of samples decreases with increase of heat-treatment temperature and this may be related to the change of domain distribution or reduction of ferromagnetic phase content (Gotardo et al., 2017). Besides, the remnant magnetization (M_r) and the coercive fields (B_c) for CLRS-2 green body are 0.21 A·m^2·kg^{-1} and 8 mT, respectively. As the heat-treatment temperature rises to 800 °C, 1000 °C and 1100 °C, M_r increases to 0.26 and 0.29 A·m^2·kg^{-1} at first, and then decreases to 0.04 A·m^2·kg^{-1}. The trend of B_c with heat-treatment temperature is the same, B_c increases to 10 and 13.7 mT at first, and then decreases to 4.6 mT. These variations and trend have been displayed in Fig. 1(b). Furthermore, the variations of saturation magnetization (M_s) and remnant coercive fields (B_{cr}), which have same trend as M_r and B_c, have also been plotted. The M_s of green body is 3.04 A·m^2·kg^{-1} which corresponds to the exsolutions in ilmenite. The decrease of B_{cr} when heat treatment temperature rose to 1100 °C may be caused by grain growth (Heider et al., 1996). For low-Ti type basalt CLRS-1, which is porous and melted at 1100 °C under vacuum (Song et al., 2019), according to Fig. 4S, the M_s of its green body is 0.44 A·m^2·kg^{-1} which is lower than that of CLRS-2. The result means that the content of ferromagnetic substance in CLRS-1 is lower than that in CLRS-2. In addition, the remanence, coercivity and hysteresis loss of CLRS-1 obviously increased after sintered at 800 °C and 1000 °C which may relate to that the magnetite gradually crystallized from complex mineral system with the increase of heat-treatment temperature (Song et al., 2019). However, the sintered samples became paramagnetic after sintered at 1100 °C. To estimate the domain state of magnetic mineral, magnetization and coercivity ratios (M_r/M_s vs. B_{cr}/B_c) was used and plotted in Fig. 1(c) according to "Day" plot (Day et al., 1977). Single domain (SD) grains are characterized by $M_{rs}/M_s > 0.5$, and $B_{cr}/B_c < 1.5$, and Multi Domain (MD) grains are characterized by $M_{rs}/M_s < 0.05$ and $B_{cr}/B_c > 4$. Pseudo-single-domain (PSD) grains are between SD and MD (Day et al., 1977). It can be seen from the Fig. 1(c) that

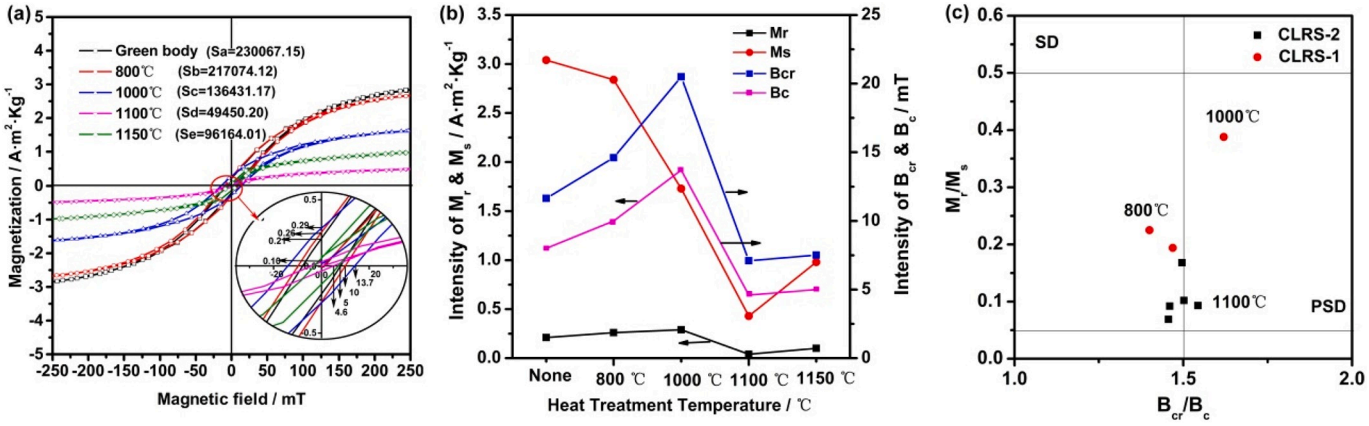

Fig. 1. Magnetic hysteresis loops of green body and sintered samples of high-Ti basalt simulated lunar regolith CLRS-2 measured at room temperature (a), in which Sa to Se in brackets that have been simplified to dimensionless value respectively represent the area of hysteresis loop corresponding to the green body and sintered sample at different temperatures. The curve of remnant magnetization (M_r), saturation magnetization (M_s), coercive fields (B_c) and remnant coercive fields (B_{cr}) of sintered samples of CLRS-2 with different sintering temperature (b). M_r/M_s vs. B_c/B_{cr} of sintered samples of CLRS-2 and CLRS-1 under different sintering temperature (c) and the inset is the enlarged view of B_{cr}/B_c between 1.4 and 1.6. "None" in the pictures on behalf of the green body which has not been heat-treated.

except for the CLRS-2 sample sintered at 1100 °C and CLRS-1 sample sintered at 1000 °C are PSD grains, all the other samples have multi-domain behavior.

3.2. Composition evolution of CLRS-2

The XRD patterns for green body and sintered samples in Fig. 2(a) indicate that crystalline phases of all samples are mainly composed of plagioclase $(Ca,Na)[(Al,Si)_4O_8]$ (PDF#99-0012 and PDF#99-0001), diopside $CaMgSi_2O_6$ (PDF#99-0045) phase and ilmenite $FeTiO_3$ (PDF#75-1208). After sintered at 800 °C and 1000 °C, the difference in the XRD patterns between sintered samples and green body is not obvious. The intensities of peaks for sample sintered at 1100 °C are generally weakened may be related to the deformation of sample and some peaks in spectrum become wider (Fig. 2(b)) which could be attributed to replacement of Ca^{2+} and Mg^{2+} by Na^{+}, Fe^{2+}, Fe^{3+} and Cr^{3+} ions (Alizadeh and Marghussian, 2000), which is consistent with the results of the Raman spectra in Figs. 5S and 6S. The peak intensity of XRD pattern of sample sintered at 1150 °C is severely weakened which may be due to smaller effective measured field caused by serious deformation and formation of porous structure as shown in Fig. 3S.

Considering the high content of ilmenite in the high-Ti type basalt simulated lunar regolith CLRS-2, the phase change of ilmenite after sintered was measured and shown in Fig. 7S. There is no obvious phase change after sintering. In addition, the measured melting point of ilmenite is 1274 °C, which is much higher than that of albite or other silicate minerals in simulated lunar regolith. Therefore, we speculate that the influence of ilmenite with higher melting point and silicate minerals with lower melting point in simulated lunar regolith on the sintering process may successively occur at different temperature.

There will be no vacuum degree change without material evaporation due to the vacuum pump rate was a constant in closed sintering chamber. Therefore, we can estimate whether there is mass loss during the sintering process of simulated lunar regolith by the change of vacuum degree of the sintering chamber. The vacuum degree variation in sintering chamber with time and temperature history in heat treatment process is shown in Fig. 3(a). During the heating stage, the vacuum degree was maintained at 5×10^{-3} mbar when the temperature below 400 °C. When heat-treatment temperature exceeded 400 °C, vacuum degree declined significantly and this downtrend continued to 550 °C, which suggests volatile substance was continuously released in this temperature range. Then, the vacuum degree ascended gradually and fluctuated between 7.5–9 $\times$ 10^{-3} mbar at a temperature range of 850–1100 °C. To clarify the effect of vacuum degree variation on sintering results, heat-treatment temperature trends to weight loss ratio and density have been measured and plotted in Fig. 3(b). The weight loss ratio increases with the increasing of heat-treatment temperature on the whole and reaches 2.41% at sintering temperature of 1150 °C, which is consistent with the result of vacuum variation which was always higher than the initial value during heating process and that means there is always mass loss during heating process. Considering the high melting point of minerals, the weight loss is mainly caused by evaporation of water adsorbed on the surface of particles or bound in lattices of secondary minerals (Kenneth et al., 2010), and glass phase with low softening point under vacuum when heat-treatment temperature is below 800 °C. However, the difference of weight loss ratio of samples under heat-treatment temperature of 800 °C and 900 °C is not significant, which can likely be attributed to the exhaustion of volatile constituents such as amorphous phase with low softening points. Then the weight loss of the samples may be caused by amorphous phase with high softening points and mineral phases when the heat-treatment temperature is higher than 900 °C (Song et al., 2019). Rising temperature can promote densification when heat-treatment temperature below 1100 °C, and sintered sample has the highest density (2.77 $g{\cdot}cm^{-3}$) when sintering temperature is 1100 °C. The density decreases to 1.86 $g{\cdot}cm^{-3}$ when sintering temperature rises to 1150 °C due to the formation of a large number of macro pores caused by massive evaporation of materials and pressure difference inside and outside pores, which has been discussed in our previous work (Kenneth et al., 2010). The trend of high-Ti type basalt simulated lunar regolith CLRS-2 during vacuum sintering process is quite similar to that of low-Ti type basalt simulated lunar regolith CLRS-1, which means that vacuum sintering of basalt-type simulated lunar regolith would successively undergo densification and macro-pore forming stages with the increase of heat-treatment temperature. However, the obvious phenomenon, which is determined by the complex components and phase of simulated lunar regolith, is rarely observed during air sintering process of simulated lunar regolith or other metal oxide ceramics.

Further analyses were carried out to confirm the composition evolution during sintering process. A comparison of the element concentrations by XRF test between green body and different sintered samples at 700 °C, 1100 °C, and 1150 °C is shown in Fig. 4. Obviously, the

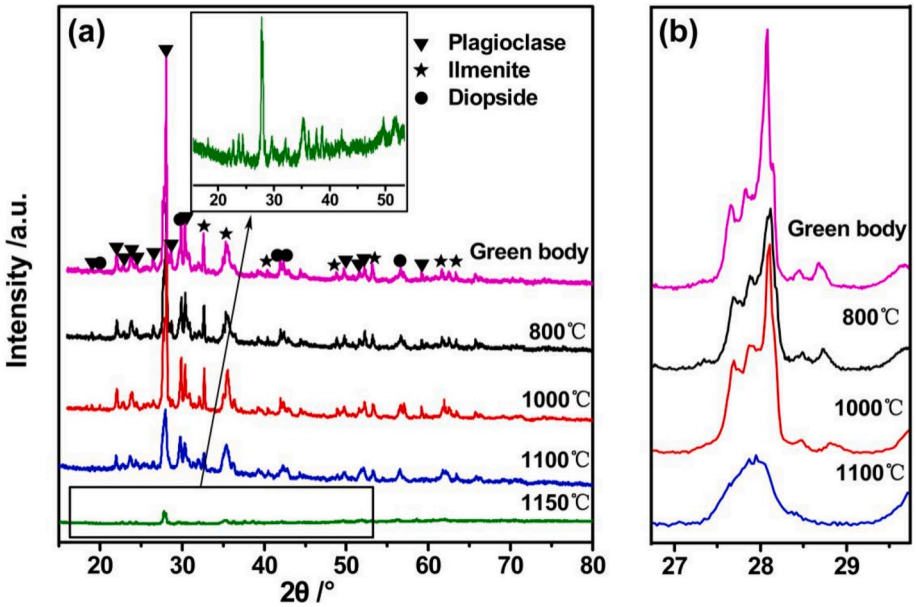

Fig. 2. The comparisons of XRD patterns of green body with CLRS-2 samples sintered at different temperatures (a) and partial enlarged detail (b).

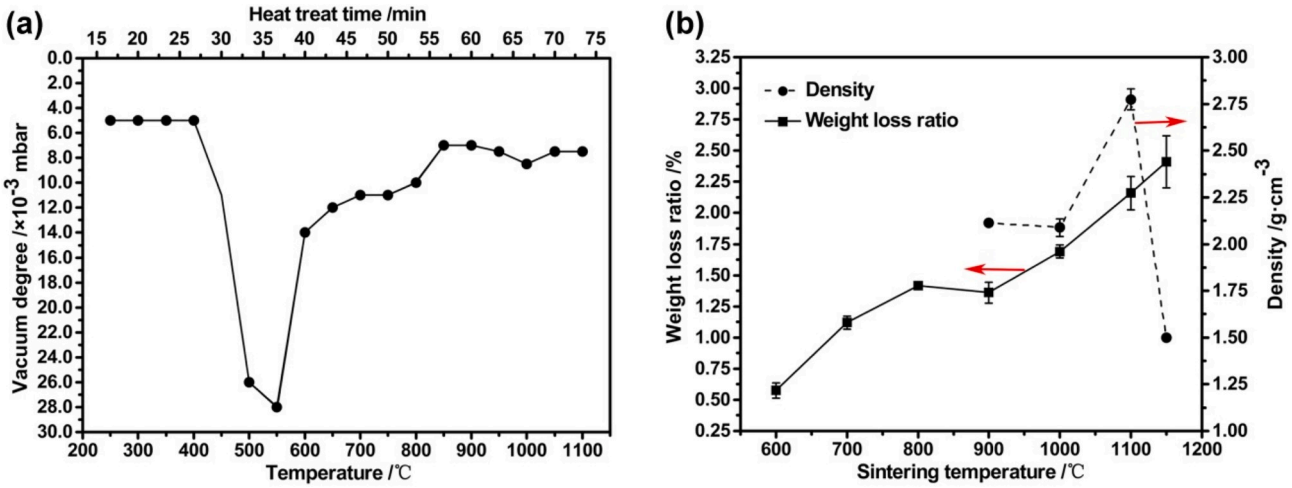

Fig. 3. The variation of vacuum degree in the sintering process for CLRS-2 sample sintered at 1100 °C (a). The weight loss ratio and the density for CLRS-2 samples sintered under different heat-treatment temperatures (b).

absolute content of each element in the sample would not increase after being vacuum-sintered, but only decrease or remain unchanged. Therefore, the increase of relative content of a component only means that there is no loss or relatively less loss of this component. For the XRF results, the apparent relative content of Si, Ca and Mg in samples has decreased while that of Fe and Ti has relatively increased after sintered at temperature no higher than 1100 °C, which may be due to ilmenite with higher melting point is quite stable at heat-treatment temperature lower than the melting point of CLRS-2, while plagioclase and other minerals with lower melting point are not as stable as ilmenite and would evaporate at high temperature in vacuum. When the sintering temperature rose to 1150 °C, the relative content of Fe and Ca greatly decreased. Meanwhile, the sample melted and a large amount of macro pores formed. As mentioned above, Fe with different valences is easy to replace other ions in minerals, which may lead to a significant decrease in the melting point of the samples in our experiments. Therefore, the results show that the composition evolution has gone through several different stages. First of all, the elements such as Mg, Si and Ca have mainly evaporated under vacuum during the densification of CLRS-2 samples (1100 °C) due to the evaporation of amorphous phase and solid solution formed by ion exchange. Then, the loss of Fe element was significantly increased at 1150 °C, which may be caused by massive evaporation of Fe-containing solid solution.

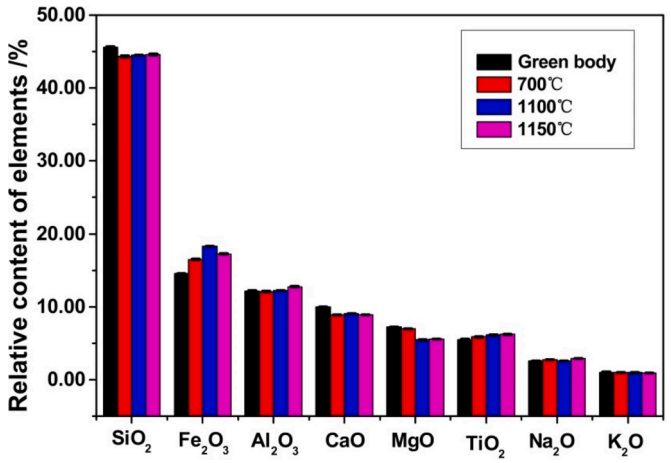

Fig. 4. Relative content of elements between CLRS-2 samples sintered at 700 °C, 1100 °C, 1150 °C and green body acquired via XRF.

3.3. Micromorphology analysis

To study the influence mechanism of ilmenite with high melting point on magnetic change in simulated lunar regolith, the morphology and elements distribution of samples were further measured by SEM and EDS. The vacuum sintered CLRS-2 and Panzhihua ilmenite samples (the source of high titanium substance in CLRS-2) at different temperatures were measured. Fig. 5 shows the characteristic SEM zones of the sample sintered at 900, 1000, 1100 and 1150 °C. No characteristic crystals were observed at other lower heat-treatment temperatures. After heat-treatment at 900 °C, octahedral-like crystals and rod-like crystals in zone A and B as shown in Fig. 5(a) were observed in local areas in sample, which could be confirmed as mainly Fe-Ti oxides according to the EDS data displayed in Table 2. Moreover, plenty of the octahedral-like crystals were also observed in sintered ilmenite samples as shown in Fig. 8S(a), which indicates that the octahedral-like crystals in Fig. 5(a) were crystallized from ilmenite composition in CLRS-2 lunar regolith simulant. The special crystals from ilmenite were observed as regular polygonal lamellar crystals stacked together in both CLRS-2 and ilmenite samples sintered at 1000 °C as shown in Fig. 5(b) and Fig. 8S(b) and no other shapes of crystals were observed. At this heat-treatment temperature, many melting zones appeared in the samples. According to EDS data at zone C, the crystal composition and element distribution are more complex. The crystals with the grain size ranges from 1 to 4 μm of samples sintered at 1100 °C are mostly regular polygonal sheet shape (Fig. 5(c)) and lath-shaped (Fig. 5(d)) which are separately Fe-Ti oxides and plagioclase phases according to the EDS data (zone D and E) and XRD results.

When heat-treatment temperature rises to 1150 °C, the grain size increased according to the contrast of Fig. 5(d) and (f), and crystals on the surface of sample can be clearly observed. Fig. 5(e) shows the magnified images of feature areas on the surface of sample sintered at 1150 °C. Unlike the sample sintered at lower temperature, the morphologies of the crystals are mainly irregular plate-like and narrow lath-shaped, and the grain size increases to 10–20 μm. According to EDS data, the plate-like and narrow lath-shaped crystals at zone G, H and J have high content of Si, Al, Na and Ca elements, indicating that the crystals are mainly composed of aluminosilicate mineral phases, namely plagioclase ($(Ca,Na)[(Al,Si)_4O_8]$) phase. Considering that there is a small amount of Mg contain in crystals, they may also contain diopside ($CaMgSi_2O_6$) phase or forsterite (Mg_2SiO_4) phase. Whereas the composition of the substance at smooth zone I is similar to crystals at zone G, H and J, but has higher content of Mg means that Mg-containing minerals in zone I are relatively higher. In addition, the content of Fe and Ti

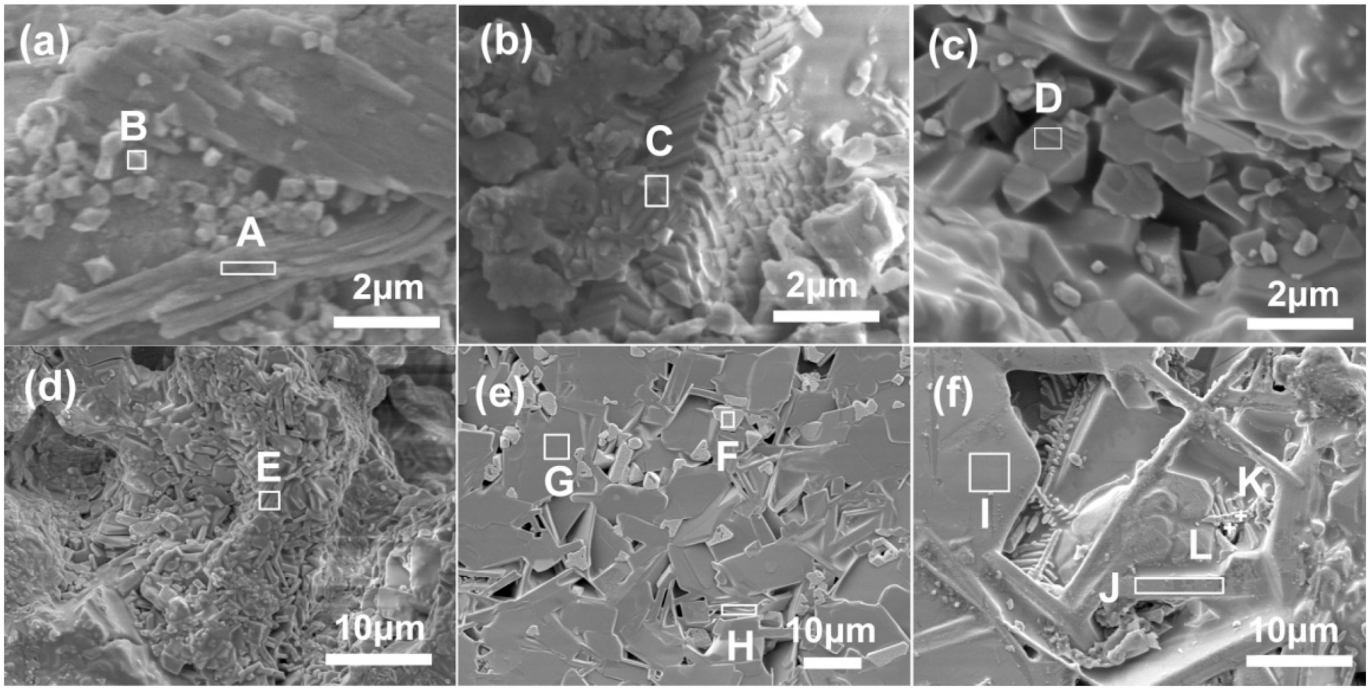

Fig. 5. Surface SEM images of magnified images of feature area of CLRS-2 samples sintered at 900 °C (a), 1000 °C (b), 1100 °C (c) (d) and 1150 °C (e) (f).

Table 2
EDS data of atom composition marked in Fig. 5.

Element	Atom/%											
	A	B	C	D	E	F	G	H	I	J	K	L
O	58.91	75.1	26.46	61.50	67.93	66.46	65.69	65.38	65.83	67.86	74.14	58.65
Na	8.74		1.39	1.25	2.47		2.81	2.61	2.37	2.82		1.31
Mg			1.25	2.03	2.92	2.91	0.64	1.12	4.42	0.5	1.6	1.41
Al			4.01	4.14	5.68	2.14	8.15	7.48	7.89	9.13	1.5	3.08
Si	0.55	0.38	7.49	8.74	15.39	0.8	12.78	15.66	14.33	15	4.61	13.62
K	0.17		0.61	0.51	0.46		0.23	0.35	0.13	0.19	0.2	0.92
Ca	1.32	0.16	3.33	1.59	3.61	0.31	2.76	4.25	2.71	3.46	1.16	3.85
Ti	11.47	8.44	10.93	4.59	0.31	5.03	1.95	1.18	0.42	0.34	6.45	7.63
Fe	18.84	15.92	44.55	15.64	1.24	22.37	4.98	1.98	1.9	0.7	10.32	9.55
Total	100	100	100	100	100	100	100	100	100	100	100	100

elements in zone F is significantly higher than that in other two zones G and H, which can be inferred that the crystals with irregular shape with relatively high content of Ti and Fe elements like crystals at zone F may crystallize from ilmenite components that mixed into the melting components due to almost complete molten of CLRS-2 sample. Furthermore, many dendrites with size of 5–10 μm were observed as shown in Fig. 5 (f). The concentrations of Fe and Ti at point K and L are much higher which means the formation of dendrites may also related to the ilmenite. Besides, the atomic ratio of Fe and Ti elements at point K and L deviates from the stoichiometric ratio of $FeTiO_3$ and the content of Fe element far higher than that of Ti element, which indicates that, after sintered at 1150 °C, ilmenite in the sample not only has phase separation, but also the Fe in ilmenite may precipitate in the form of dendrites.

3.4. Micro-hardness of samples

As a physical property of material, micro-hardness reflects the resistance to plastic deformation. Thus, micro-hardness of two simulated lunar regolith sintered at 1100 °C and 1150 °C under vacuum has been measured and listed in Table 3 that of samples sintered at lower temperature was not measured because the un-bonded particles lead to samples could not be polished. There is an apparent difference among hardness values at different points which demonstrates the inhomogeneous distribution of components in samples. Whereas the difference is not obvious between two types of simulated lunar regolith at the same heat-treatment temperature, indicating that the different compositions for CLRS-1 and CLRS-2 may have small influence on the micro-hardness of sintered simulated lunar regolith, which may be mainly related to sample sintering state and density. Besides, the micro-hardness of all sintered samples is much higher than that of 3D printing JSC-1 samples reported by Goulas et al. (Goulas and Friel, 2016), which may due to our conventional sintered samples have higher density. The results demonstrated that the ilmenite content difference have no

Table 3
Vickers-hardness of CLRS-1 and CLRS-2 samples sintered at 1100 °C and 1150 °C under vacuum.

Sintering temperature/°C	Vickers-hardness/HV	
	CLRS-1	CLRS-2
1100	733.89	668.47
	675.31	802.70
	822.97	715.99
1150	885.13	764.97
	782.08	909.63
	853.42	857.75

influence on the micro-hardness of samples. However, the density of samples and the sintering condition such as temperature have a greater influence. These results tell us the hardness of sintered basalt type lunar simulants has a tolerance to the composition difference, which is quite encouraging for lunar regolith forming technology and the application of building materials.

4. Discussions

Combining the SEM results of vacuum sintered CLRS-2 samples and ilmenite samples, we can conclude that the crystallization behaviors of ilmenite in the two powder sample systems are different. For Panzhihua ilmenite powder system, octahedral-like crystals were observed at lower heat-treatment temperature (≤1000 °C), and then the octahedral-like crystals grew up with increasing temperature and developed into relatively complete hexagonal flake crystals at 1100 °C. A large number of irregular crystals of different shapes and sizes appeared in the samples sintered at 1150 °C, which was lower than the measured melting point (1274 °C) of ilmenite. The crystallization variation of ilmenite in CLRS-2 was the same as that of ilmenite in Panzhihua ilmenite powder at heat-treatment temperature no higher than 1100 °C. However, when the sintering temperature for CLRS-2 rose to 1150 °C, ilmenite components mixed into the melting components due to almost complete molten of mineral phase and amorphous phase in CLRS-2 sample, and then crystallized in form of dendrite crystals and crystals at zone F in Fig. 5(e). Obviously, ilmenite component with higher melting point in CLRS-2 has an important influence on its sintering process, while the various components such as plagioclase and amorphous phase in lunar regolith would in turn affect the sintering behavior of ilmenite. This further confirms that the particularity of sintering of lunar regolith under vacuum conditions and its evolution of each components deserve further exploration.

According to the morphology and composition evolution analysis, the surface morphology of the sample change with the increase of heat treatment temperature to no higher than 1000 °C, the crystal shape and grain size in samples are different and surface enrichments of Fe-containing compounds are similar at different temperature. Thus, the minor magnetic property difference between green body and samples sintered at 800 °C and 1000 °C may arise from the change of morphology, size or distribution of ferromagnetic phase crystals (Forster, 1973). When temperature rose up to 1100 °C, the grain size increased, new crystals and solid solutions began to appear in large quantities and the trend of Fe enrichment on the surface was weakened. Hence, the significant reduction of M_r and B_c of sample sintered at 1100 °C could be explained by the grain growth and the reduction of ferromagnetic phase content which caused by replacement of Ca^{2+} and Mg^{2+} in plagioclase by Fe^{2+} and Fe^{3+} ions in ilmenite. The morphologies of samples sintered at 1150 °C differed greatly. The components containing Si, Mg, Ca and other elements melted a lot, and new crystals with very large grain size emerged. Meanwhile, Fe-containing compounds mainly existed in the form of precipitated new crystals and dendrites, and the decrease of grain size and morphological changes may lead to increase of M_r and B_c. As studies in our previous work, the CLRS-1 samples sintered in vacuum have a continuously Fe_3O_4 crystal creation and new crystals emerge above 1000 °C, the crystals further change at 1100 °C. Thus, the magnetic enhancement of CLRS-1 simulated lunar regolith after heat treatment may due to a large amount of magnetite crystallization. When the heat treatment temperature rose to 1100 °C, the sample melted and reactions including solid solution and ions replacement occurred, which destroy the domain of magnetite. Thus the sample shows paramagnetism which is attributed to paramagnetic minerals such as pyroxene and olivine.

5. Conclusions

This study investigated the relationship between composition evolution and magnetic property of high-Ti type basalt CLRS-2 lunar simulant during sintering processing under vacuum by comparing with that of ilmenite and reported low-Ti type basalt CLRS-1 sintered in vacuum. The results show that effects of ilmenite and magnetite on the evolution of composition, micro-morphology and magnetic properties of simulated lunar regolith during sintering process are different. When heat-treatment temperature lower than melting point of simulated lunar regolith, the ferromagnetism of the simulated lunar regolith CLRS-1 containing ferromagnetic magnetite strengthened after being heat treated, while that of the simulated lunar regolith CLRS-2 containing more antiferromagnetic ilmenite become weaker, under the influence of a large amount of paramagnetic substrates before simulated lunar regolith melting. Whereas when heat-treatment temperature higher than the melting point of the simulated lunar regolith, CLRS-1 become paramagnetism which means the domain of ferromagnetic component was destroyed by reactions among minerals at high temperatures. However, the ferromagnetism of CLRS-2 strengthened due to the change of crystalline morphology of ilmenite. The above results imply that ions substitution between ilmenite and other minerals or amorphous phase would occur at high temperature in vacuum, which would lead to the evaporation of Fe-containing components and the formation of dendrites. However, whether will the ilmenite form dendrites, which have an adverse effect on mechanical property of sintered samples (He et al., 2004), in real lunar regolith need to be further explored. Furthermore, in consideration of the valence differences of iron-containing substances between simulated and real lunar soils, the effect of lower-valent Fe-containing components on sintering process for lunar regolith need to be explored. In addition, the results show that when using Martian regolith to prepare magnetic ceramics/glass by conventional sintering, it may be necessary to strictly control the temperature to prevent the domain from being damaged by high temperature reaction. Finally, the micro-hardness of CLRS-1 and CLRS-2 sintered samples was measured, the results show that the hardness values of the same sample vary greatly at different points and that of the two simulated lunar regolith at the same heat-treatment temperature are similar, which indicates that the ilmenite content difference have no influence on the micro-hardness of the sintered samples, while the density of samples and the sintering condition such as temperature have a greater influence. These results will be helpful to improve the sintering process of lunar regolith on Moon.

Declaration of competing interest

The authors declare no competing interests.

Acknowledgements

This work was financially supported by the National Natural Science Foundation of China, China (No. 51302309), the Strategic Pioneer Program on Space Science, Chinese Academy of Sciences, China (Grant no. XDA15013700) and the Key Research Program of Chinese Academy of Sciences, China (Grant no. ZDRW-KT2016-1).

Author contributions

J.X. conceived and designed the project. H.T., X.L. and J.L. fabricated the lunar regolith simulants. L.S. carried out the sintering experiments. S.F. and J.X. supervised the experiments. L.S. carried out all the characterization experiments and discussed with J.X. and H.T.. L.S. and J.X. co-wrote the paper. All the authors discussed the results.

Appendix A. Supplementary data

Supplementary data to this article can be found online at https://doi.org/10.1016/j.icarus.2020.113810.

References

Alizadeh, P., Marghussian, V.K., 2000. The effect of compositional changes on the crystallization behaviour and mechanical properties of diopside-wollastonite glass-ceramics in the $SiO_2 \pm CaO \pm MgO$ (Na_2O) system. J. Eur. Ceram. Soc. 20, 765–773.

Bischoff, A., Rubin, A.E., Keil, K., Strffler, D., 1984. Lithification of gas-rich chondrite regolith breccias by grain boundary and localized shock melting. Earth Planet. Sc. Lett 66 (1–3), 1–10.

Coey, J.M.D., Mørup, S., Madsen, M.B., Knudsen, J.M., 1990. Titanomaghemite in magnetic soils on Earth and Mars. J. Geophys. Res-Sol Ea. 95 (B9), 14423.

Colson, R., Haskin, L., 1992. Oxygen from Lunar Soil by Molten Silicate Electrolysis, 3. NASA, Johnson Space Center, Space Recourses, pp. 195–209.

Crawford, I.A., 2015. Lunar resources: a review. Prog. Phys. Geogr. 39 (2), 137–167.

Day, R., Fuller, M., Schmidt, V.A., 1977. Hysteresis properties of titanomagnetites: grain-size and compositional dependence. Phys. Earth Planet. Inter. 13 (4), 260–267.

Forster, D.W., 1973. Mössbauer search for ferric oxide phases in lunar materials and simulated lunar materials. In: Fourth Lunar Science Conference, Houston, Texas, pp. 2697–2707.

Garrick-Bethell, I., Weiss, B.P., 2010. Kamacite blocking temperatures and applications to lunar magnetism. Earth Planet. Sc. Lett. 294 (1–2), 1–7. https://doi.org/10.1016/j.epsl.2010.02.013.

Goldstein, J.I., Scott, E.R.D., Chabot, N.L., 2009. Iron meteorites: crystallization, thermal history, parent bodies, and origin. Geochemistry 69 (4), 293–325. https://doi.org/10.1016/j.chemer.2009.01.002.

Gotardo, R.A.M., Silva, E.F.R., Montanher, D.Z., Santos, G.M., Silva, K.L., Cótica, L.F., Santos, I.A., Guo, R., Bhalla, A.S., 2017. Improved magnetic properties and structural characterizations in Mn doped $0.9BiFeO_3$–$0.1BaTiO_3$ compositions. Scripta Mater 130, 161–164. https://doi.org/10.1016/j.scriptamat.2016.11.034.

Goulas, A., Binner, J.G.P., Engstrøm, D.S., Harris, R.A., Friel, R.J., 2019. Mechanical behaviour of additively manufactured lunar regolith simulant components. Proceedings of the Institution of Mechanical Engineers, Part L: Journal of Materials: Design and Applications 233 (8), 1629–1644. https://doi.org/10.1177/1464420718777932.

Goulas, A., Friel, R.J., 2016. 3D printing with moondust. Rapid Prototyp. J. 22 (6), 864–870. https://doi.org/10.1108/rpj-02-2015-0022.

Gustafson, R., White, B., Fidler, M., 2009. Demonstrating carbothermal reduction of lunar regolith using concentrated solar energy. In: AIAA Space 2009 Conference & Exposition, Pasadena, California. https://doi.org/10.2514/6.2009-6476.

Hargraves, R.B., Collinson, D.W., Arvidson, R.E., Cates, P.M., 1979. Viking magnetic properties experiment: extended mission results. J. Geophys. Res-Sol Ea. 84.

He, G., Hagiwara, M., Eckert, J., 2004. Effect of Sn on microstructure and mechanical properties of Ti-base dendrite/ultrafine-structured multicomponent alloys. Metall. Mater. Trans. A 35 (11), 3605–3612.

Heider, F., Zitzelsberger, A., Fabian, K., 1996. Magnetic susceptibility and remanent coercive force in grown magnetite crystals from 0.1 μm to 6 mm. Phys. Earth Planet. Inter. 93 (3–4), 239–256.

Hintze, P.E., Quintana, S., 2013. Building a lunar or martian launch pad with in situ materials: recent laboratory and field studies. J. Aerospace Eng. 26 (1), 134–142. https://doi.org/10.1061/(asce)as.1943-5525.0000205.

Hoffmann, A., 2004. Symmetry driven irreversibilities at ferromagnetic-antiferromagnetic interfaces. Phys. Rev. Lett. 93 (9), 097203 https://doi.org/10.1103/PhysRevLett.93.097203.

Hong, B., Fu, W., Liu, F., 2012. Research on decomposition structure and magnetic property of ilmenite solid solution. Multipurpose Utilization of Mineral Resources 6, 22–24,32.

Kawamoto, H., Shirai, K., 2012. Electrostatic transport of lunar soil for in situ resource utilization. J. Aerospace Eng. 25 (1), 132–138. https://doi.org/10.1061/(asce)as.1943-5525.0000094.

Kenneth, J., Street, W., Ray, C., Rickman, D., Scheiman, D.A., 2010. Thermal properties of lunar regolith simulants. In: Eng. Sci. Constr. Oper. Challenging Environ. 12th Earth Sp, pp. 266–275.

Li, C., Liu, D., Liu, B., Ren, X., Liu, J., He, Z., Zuo, W., Zeng, X., Xu, R., Tan, X., Zhang, X., Chen, W., Shu, R., Wen, W., Su, Y., Zhang, H., Ouyang, Z., 2019. Chang'E-4 initial spectroscopic identification of lunar far-side mantle-derived materials. Nature 569 (7756), 378–382. https://doi.org/10.1038/s41586-019-1189-0.

Meurisse, A., Makaya, A., Willsch, C., Sperl, M., 2018. Solar 3D printing of lunar regolith. Acta Astronaut. https://doi.org/10.1016/j.actaastro.2018.06.063.

Nagata, T., Ishikawa, Y., Kinoshita, H., Kono, M., Syono, Y., Fisher, R.M., 1970. Magnetic properties and natural remanent magnetization of lunar materials, proceedings of the Apollo 11 Lunar Science Conference. Cosmochimica Acta 2325–2340.

Nagata, T., Fisher, R.M., Schwerer, F.C., Fuller, M.D., Dunn, J.R., 1971. Magnetic properties and remanent magnetization of Apollo 12 lunar materials and Apollo 11 lunar microbreccia. In: Lunar & Planetary Science Conference, pp. 2461–2476.

Ramachandran, N., Ray, C.S., Rogers, J.R., 2004. Developing glassy magnets from simulated composition of Martian soil for exploration applications. MRS Proc. 851 (33), 17–20. https://doi.org/10.1557/PROC-851-NN10.5.

Rochette, P., Gattacceca, J., Ivanov, A.V., Nazarov, M.A., Bezaeva, N.S., 2010. Magnetic properties of lunar materials: meteorites, Luna and Apollo returned samples. Earth Planet. Sc. Lett. 292 (3–4), 383–391. https://doi.org/10.1016/j.epsl.2010.02.007.

Schreiner, S.S., Dominguez, J.A., Sibille, L., Hoffman, J.A., 2016. Thermophysical property models for lunar regolith. Adv. Space Res. 57 (5), 1209–1222. https://doi.org/10.1016/j.asr.2015.12.035.

Slyuta, E.N., 2014. Physical and mechanical properties of the lunar soil (a review). Solar Syst. Res. 48 (5), 358–382. https://doi.org/10.1134/s0038094614050050.

Song, L., Xu, J., Fan, S., Tang, H., Li, X., Liu, J., Duan, X., 2019. Vacuum sintered lunar regolith simulant: pore-forming and thermal conductivity. Ceram. Int. 45 (3), 3627–3633. https://doi.org/10.1016/j.ceramint.2018.11.023.

Taylor, L.A., Meek, T.T., 2004. Microwave processing of lunar soil. Adv. Astronaut. Sci. 108, 109–123.

Taylor, L.A., Pieters, C.M., Britt, D., 2016. Evaluations of lunar regolith simulants. Planet. Space Sci. 126, 1–7. https://doi.org/10.1016/j.pss.2016.04.005.

Williams, R.J., Gibson, E.K., 1972. The origin and stability of lunar goethite, hematite and magnetite. Earth Planet. Sc. Lett. 17 (1), 0–88.

Yang, J., Zhenrong, S., Zhaolong, D., Qiong, W., Zhuo, T., 2014. Lunar soil simulant and its engineering application in lunar exploration program. Spacecr. Environ. Eng. 31 (3), 241–247. https://doi.org/10.3969/j.issn.1673-1379.2014.03.002.

Zheng, Y., Ouyang, Z., Wang, S., Zou, Y., 2004. Physical and mechanical properties of lunar regolith. J. Mineral. Petrol. 24, 14–19.